Pacific Northwest
NATIONAL LABORATORY

PNNL-33229

Focusing Ions at Atmospheric Pressure using Nonlinear DC Voltage Sequences Applied to a Stacked Ring Ion Guide

September 2022

Adam L. Hollerbach
Yehia M. Ibrahim
Randolph V. Norheim
Thomas O. Metz
Robert G. Ewing

U.S. DEPARTMENT OF ENERGY

Prepared for the U.S. Department of Energy
under Contract DE-AC05-76RL01830

DISCLAIMER

PACIFIC NORTHWEST NATIONAL LABORATORY
operated by
BATTELLE
for the
UNITED STATES DEPARTMENT OF ENERGY
under Contract DE-AC05-76RL01830

Printed in the United States of America

Available to DOE and DOE contractors from the Office of Scientific and Technical Information,
P.O. Box 62, Oak Ridge, TN 37831-0062
www.osti.gov
ph: (865) 576-8401
fax: (865) 576-5728
email: reports@osti.gov

Available to the public from the National Technical Information Service
5301 Shawnee Rd., Alexandria, VA 22312
ph: (800) 553-NTIS (6847)
or (703) 605-6000
email: info@ntis.gov
Online ordering: http://www.ntis.gov

PNNL-33229

Focusing Ions at Atmospheric Pressure using Nonlinear DC Voltage Sequences Applied to a Stacked Ring Ion Guide

September 2022

Adam L. Hollerbach
Yehia M. Ibrahim
Randolph V. Norheim
Thomas O. Metz
Robert G. Ewing

Prepared for
the U.S. Department of Energy
under Contract DE-AC05-76RL01830

Pacific Northwest National Laboratory
Richland, Washington 99354

Summary

A new technique was developed for focusing ions at elevated pressures, including atmospheric pressure. To perform the technique, DC voltage gradients that followed quadratic and exponential (power) mathematical functions were applied to a 10-cm long stacked ring ion guide instead of the conventionally used linear sequences. Both nonlinear voltage gradients caused ions to focus to the center of the ion guide in simulations and experiments. The quadratic gradient showed modest ion focusing effects while the power sequence showed strong ion focusing effects, albeit with some ion losses. This is the first demonstration of ions being focused at atmospheric pressure using nonlinear DC voltage gradients, and the results shown in this study deviate from the current understanding that RF must almost exclusively be used to focus and confine ions.

Acknowledgments

We would like to thank Professor John M. Hollerbach for helpful discussions involving mathematical derivations and data analysis. This research was supported by the M/Q initiative, under the Laboratory Directed Research and Development (LDRD) Program at Pacific Northwest National Laboratory (PNNL). PNNL is a multi-program national laboratory operated for the U.S. Department of Energy (DOE) by Battelle Memorial Institute under Contract No. DE-AC05-76RL01830.

Contents

Figures

Tables

1.0 Introduction

One of the great challenges in analytical chemistry is effectively confining small ions over long distances at atmospheric pressure (AP). There are many potential applications of an effective AP ion confinement method, such as providing shorter deposition times and wider deposition areas for AP soft-landing (Badu-Tawiah, Wu, and Cooks, 2011, 2648-2654; Tata, Salvitti, and Pepi, 2020, 116309). Ion confinement is conventionally performed at low pressure (< 10 Torr) using high voltage radiofrequencies (RF). Many analytical instruments and ion optics utilize RF, including ion mobility spectrometry (IMS), mass spectrometry (MS), quadrupole mass filters (Douglas, 2009, 937-960), ion traps (Nolting, Malek, and Makarov, 2019, 150-168), RF-confining drift tubes (Bush et al., 2010, 9557-9565; Allen and Bush, 2016, 2054-2063), ion funnels (Shaffer et al., 1997, 1813-1817), traveling wave ion mobility spectrometers (TWIMS) (Shvartsburg and Smith, 2008, 9689-9699), and structures for lossless ion manipulations (SLIM) (Deng et al., 2016, 8957-8964; Deng et al., 2017, 4628-4634). However, standard RF conditions are not sufficient to overcome ion diffusion effects at AP, and the RF conditions needed to establish AP ion confinement are not easily implemented or practical (i.e., the breakdown potential of air will be reached well before such conditions are achieved). To date, no methods employing electrostatic lenses can focus ions at AP with the same effectiveness that RF does at lower pressures, and there remains a substantial knowledge gap in alternative ion focusing techniques.

Most existing AP ion focusing and ion confinement methods utilize electrostatic focusing lenses, gas dynamics, or both (Kolomiets and Pervukhin, 2011, 1792-1797; Garimella et al., 2012, 201-207; Kottke et al., 2017, 8981-8987; Zhou et al., 2003, 5978-5983). It is attractive to use electrostatic lenses to manipulate ions at AP because they are relatively straightforward to construct and operate. Several studies have reported on ion focusing effects over short distances using single electrostatic lenses. For example, it was possible to generate collimated ESI droplet plumes by applying high voltages to single ring electrodes placed in front of electrospray and paper-spray ionization sources, which resulted in improved MS signal intensities and detection limits (Salentijin, Oleschuk, and Verpoorte, 2017, 11419-11426; Smith et al., 2022, 116737; Schneider, Douglas, and Chen, 2002, 906-913). Alternatively, a single electrostatic lens with an ellipsoidal geometry was used to focus ESI-generated ions at AP to an MS inlet, which resulted in up to 4x improved signal intensities. However, some pneumatic assistance helped direct charged droplets and ions (Baird, Peng, and Cooks, 2012, 277-284).

A few studies report on AP ion focusing effects over long distances, which usually requires several closely spaced electrostatic lenses (e.g., stacked ring ion guide). Meier and coworkers (2021, 2076-2080) placed a conventional ion funnel (i.e., stacked ring electrodes with decreasing inner diameter, DC+RF voltages) in front of an MS capillary inlet and showed a 1000x improvement in detection limits from an extractive ESI source compared to when no ion funnel was present. The improvement was predominantly from the presence of a DC voltage and the geometries of the ring electrodes themselves since RF has been demonstrated to be ineffective at pressures above ~30 Torr for conventional ion funnels (Ibrahim et al., 2006, 1299-1355; Kelly et al., 2010, 294-312). Alternatively, 3D printed conductive plastic electrodes with curved geometries (e.g. U-turns, 90° bends, S-shapes) have been used to demonstrate ion transmission over ~10 cm effective path lengths when using linear voltage gradients (Baird, Wei, and Cooks, 2015, 696-700; Iyer et al., 2019, 2584-2593; Schrader, Marsh, and Cooks, 2020, 116391). Understandably, narrower ion mobility peaks were obtained when curved devices were comprised of many thin electrodes with small spacings, leading to greater electric

field homogeneity compared to the same device comprised of thicker electrodes or electrodes spaced far apart (Schrader, Marsh, and Cooks, 2020, 116391).

Compared to AP, several alternatives to RF confinement using electrostatic focusing lenses operate in the low pressure regime (~1 Torr). Russell and coworkers (Gillig, Ruotolo, Stone, and Russell, 2004, 43-49; Fort, Silveira, and Russell, 2013, 9543-9548) explored a periodic ion focusing effect (at ~1 Torr) where ions with an initial momentum iteratively focus and defocus (also accelerate and decelerate, respectively) as they propagate through a conventional stacked ring ion guide or ion funnel comprised of thick ring electrodes (~4-6 mm) spaced relatively far apart (~6 mm). The effectiveness of such a device at AP is unknown due to significantly increased dampening effects at higher pressures. Alternatively, Anthony and coworkers (2014, 1-7) placed a DC-only ion carpet (i.e., a single plate consisting of closely spaced concentric rings) at the end of a drift tube in an attempt to overcome the need to use RF. Applying a linear voltage sequence to the ion carpet resulted in upwards of 90% ion transmission with little mobility discrimination while applying an unspecified nonlinear voltage sequence resulted in a more spatially focused ion beam.

To date there does not appear to be any study that combines electrostatic lenses and nonlinear voltage sequences to focus ions at AP in a 3D space (i.e., along a drift tube). Nonlinear voltage sequences (e.g., quadratic sequence) have been applied to reflectrons in TOF-MS systems to refocus ions possessing small differences in kinetic energy, but TOF-MS systems require high-vacuum (< 10-6 Torr) and it is currently unclear if such a process is translatable to AP (Mächler, Filippov, and Derrick, 2015, 115-123).

In this study we describe a new methodology for focusing ions in 3D at AP by applying a nonlinear series of DC voltages to a stacked ring ion guide. We performed a rigorous set of simulations to demonstrate ion focusing effects using quadratic and power (exponential) voltage sequences and show that curved electric field lines are generated due to the constantly changing voltages. We spatially map ion distributions using a segmented Faraday cup detector to validate the results of the simulations and show that ion currents are increased when using nonlinear voltage gradients to focus ions at AP.

2.0 Experimental Details

2.1 Ion Trajectory Simulations

Simulations were performed using SIMION 8.1 incorporating the statistical diffusion simulation (SDS) collision model. Each simulation utilized 10,000 ions per experiment (1000 ions per run, 10 runs, m/z 130, 2e-12 C space charge per run). The simulated stacked ring ion guide consisted of 100 electrodes (25.4 mm i.d., 0.5 mm thickness) spaced 0.5 mm apart. A small ion emitter (3 mm length, 1 mm o.d.) was placed at the front of the electrode stack to mimic an ESI tip. A focusing electrode (8.5 mm length, 50 mm i.d.) was placed in front of the electrode stack to guide ions into the stacked ring electrodes. The emitter and focusing electrode were held at +2500 and +500 V above the voltage applied to the first ring electrode, respectively. A collection plate was placed at the end of the stacked ring ion guide and held at + 15 V. The simulated buffer gas was 760 Torr nitrogen.

2.2 Chemicals and Electrospray Ionization

Seven tetraalkylammonium salts (TAA_C_2 – TAA_C_8) were purchased from Millipore-Sigma (St. Louis, MO, USA) as either the chloride, bromide, or hydrate salts. The TAA salts were dissolved in acetonitrile and diluted to 10 µM. NanoESI emitters (2-4 µm o.d.) were pulled from borosilicate glass capillaries (10 cm length, 1.5 mm o.d., 0.86 mm i.d.) using a P-2000 laser tip puller (Sutter Instruments, Novato, CA, USA). High voltage was applied to the solutions via a stainless-steel wire inserted into a microelectrode holder (Warner Instruments, Hamden, CT, USA).

2.3 Instrumentation and Electronics

A schematic of the experimental setup used to validate the simulations is shown in Figure 1A. A PCB-based stacked ring ion guide (10 cm length) was constructed using FR-4 material with copper plated electrodes. Each plate containing the electrodes was 0.5 mm x 41.3 mm x 41.3 mm (L x W x H). Three voltage divider circuits (linear, quadratic, and power) were constructed by soldering resistors onto custom PCBs. All resistors possessed a 1% tolerance, and a list of the resistors used for each circuit is given in the Supporting Information (Table 1). Two 50-wire ribbon cables were used to connect the PCBs to the ring electrodes.

2.4 Concentric ring Faraday detector

A Faraday detector comprised of 21 concentric rings was designed and constructed to provide spatially distributed ion current measurements. Similar detectors with a concentric ring design have been reported elsewhere (Karpas et al., 1993, 95-104). A schematic of the concentric ring detector used in the present study are shown in Figure 1D. A 1 mm diameter pad was located in the center of the detector. Concentric rings were spaced 0.14 mm apart and possessed widths of 0.5 mm. The length of the detector plate was 1.725” to allow for electrical connections to be soldered. An electrical circuit employing a 3-pin header and 21 jumper shunts was constructed and attached to the reverse side of the detector (Figure 1E). This circuit allowed ion current from any number of rings to be measured by moving the jumper shunts from one side of the circuit to the other. Connecting all 21 rings together allowed the detector to function as a typical Faraday cup. Ion currents were measured using a Keithley 428 current amplifier (Cleveland, OH, USA) connected to a Tektronix DPO 5204B oscilloscope (Beaverton, OR, USA). Each voltage divider circuit was connected or to a 9V battery through a

1MOhm resistor because the battery provided much less noise than grounding through the power supply. The Faraday cup detector, detection circuit, voltage divider circuits, and wiring were shielded with grounded aluminum foil to eliminate interference from laboratory noise and mains power (i.e., 60 Hz).

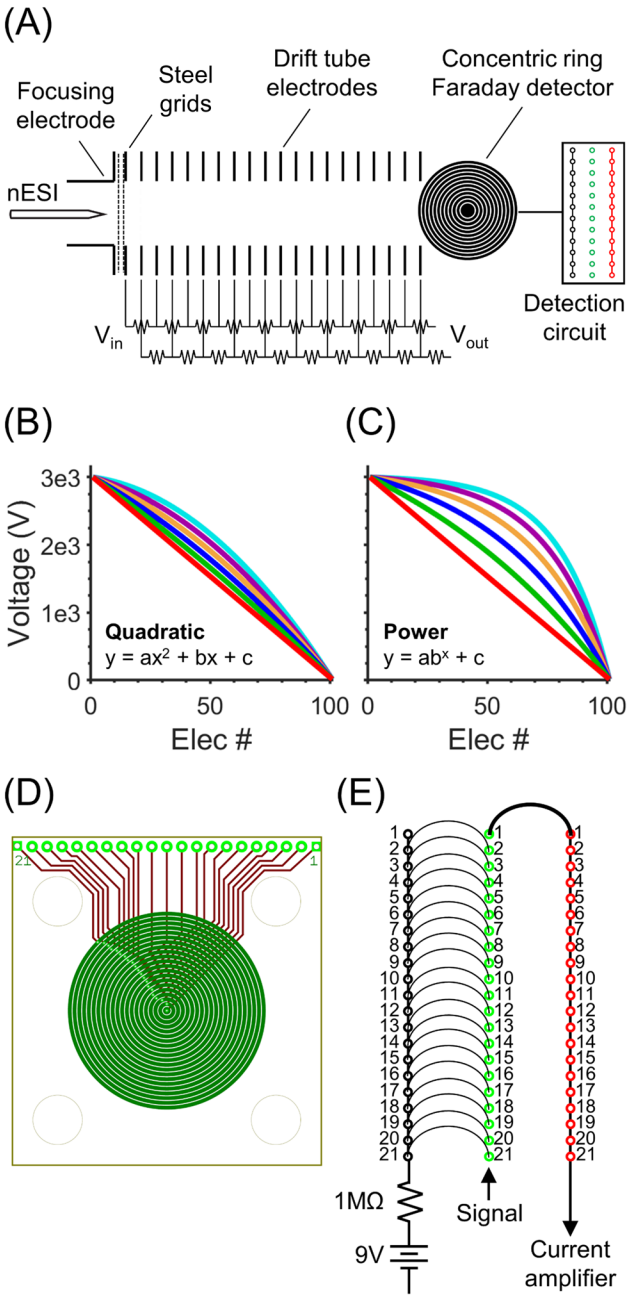

Figure 1: (A) Experimental schematic of a stacked ring ion guide with a focusing electrode, voltage divider circuits, Faraday cup detector comprised of 21 concentric rings, and an ion current detection circuit. (B,C) Curves of voltages applied to 100 ring electrodes that follow quadratic and power functions with six different incr values (quadratic = 0.0,0.1,0.2,0.3,0.4,0.5; power = 1.00,1.01,1.02,1.03,1.04,1.05). (D) Schematic of the concentric ring Faraday cup detector used to spatially map ion distributions at the end of the stacked ring ion guide. (E) Schematic of the ion current detection circuit used alongside the concentric ring Faraday cup detector.

Table 1: Resistor values used to construct linear, quadratic (0.5), and power (1.05) voltage divider circuits. Actual resistances used are multiplied by 1000.

	Linear	Quadratic	Power
Resistor #	--	Incr = 0.5	Incr = 1.05
1 / 51	100 / 100	16.9 / 100	3.83 / 44.2
2 / 52	100 / 100	18.7 / 102	4.02 / 46.4
3 / 53	100 / 100	20.5 / 105	4.22 / 48.7
4 / 54	100 / 100	22.1 / 105	4.42 / 51.1
5 / 55	100 / 100	23.7 / 107	4.64 / 53.6
6 / 56	100 / 100	25.5 / 110	4.87 / 56.2
7 / 57	100 / 100	26.7 / 110	5.11 / 59.0
8 / 58	100 / 100	28.7 / 113	5.36 / 61.9
9 / 59	100 / 100	30.1 / 113	5.62 / 64.9
10 / 60	100 / 100	31.6 / 115	5.90 / 68.1
11 / 61	100 / 100	34.0 / 118	6.19 / 71.5
12 / 62	100 / 100	35.7 / 118	6.49 / 75.0
13 / 63	100 / 100	37.4 / 121	6.81 / 78.7
14 / 64	100 / 100	38.3 / 121	7.15 / 82.5
15 / 65	100 / 100	40.2 / 124	7.50 / 86.6
16 / 66	100 / 100	42.2 / 124	7.87 / 90.9
17 / 67	100 / 100	43.2 / 127	8.25 / 95.3
18 / 68	100 / 100	45.3 / 130	8.66 / 100
19 / 69	100 / 100	47.5 / 130	9.09 / 105
20 / 70	100 / 100	48.7 / 133	9.53 / 110
21 / 71	100 / 100	49.9 / 133	10.2 / 115
22 / 72	100 / 100	52.3 / 137	10.7 / 121
23 / 73	100 / 100	53.6 / 137	11.3 / 127
24 / 74	100 / 100	54.9 / 140	11.8 / 133
25 / 75	100 / 100	57.6 / 140	12.4 / 140
26 / 76	100 / 100	59.0 / 143	13.0 / 147
27 / 77	100 / 100	60.4 / 143	13.7 / 154
28 / 78	100 / 100	61.9 / 147	14.3 / 162
29 / 79	100 / 100	63.4 / 147	15.0 / 169
30 / 80	100 / 100	64.9 / 150	15.8 / 178
31 / 81	100 / 100	66.5 / 150	16.5 / 187
32 / 82	100 / 100	68.1 / 154	17.4 / 200
33 / 83	100 / 100	69.8 / 154	18.2 / 210
34 / 84	100 / 100	71.5 / 154	19.1 / 221
35 / 85	100 / 100	73.2 / 158	20.0 / 232
36 / 86	100 / 100	75.0 / 158	21.0 / 243
37 / 87	100 / 100	76.8 / 162	22.1 / 255
38 / 88	100 / 100	78.7 / 162	23.2 / 267
39 / 89	100 / 100	80.6 / 165	24.3 / 280
40 / 90	100 / 100	82.5 / 165	25.5 / 294
41 / 91	100 / 100	84.5 / 165	26.7 / 309
42 / 92	100 / 100	84.5 / 169	28.0 324
43 / 93	100 / 100	86.6 / 169	29.4 / 340
44 / 94	100 / 100	88.7 / 174	30.9 / 357
45 / 95	100 / 100	90.9 / 174	32.4 / 374
46 / 96	100 / 100	90.9 / 174	34.0 / 392
47 / 97	100 / 100	93.1 / 178	35.7 / 412
48 / 98	100 / 100	95.3 / 178	37.4 / 432
49 / 99	100 / 100	97.6 / 182	39.2 / 453
50 / 100	100 / 100	97.6 / 182	41.2 / 475

3.0 Results and Discussion

3.1 Generation of quadratic and power function voltage sequences

Traditional stacked ring ion guides typically employ linear voltage sequences to facilitate ion transfer across the drift region. Each successive ring electrode possesses an incrementally lower voltage than the previous electrode (e.g. 1000 V, 990 V, 980 V, 970 V, etc.). While linear voltage sequences are straightforward to implement, they do not provide any mechanism to confine ions. This lack of confinement limits the maximum length that an AP stacked ring ion guide can be before substantial ion losses occur.

To overcome ion losses at AP, we studied the effects of applying nonlinear voltage sequences to 100 ring electrodes placed in a stacked ring ion guide arrangement. We evaluated two nonlinear functions in this study: (1) quadratic and (2) power (exponential) functions (Figure 1B, Figure 1C). The quadratic sequence follows a standard quadratic equation ($y = ax^2 + bx + c$) described by equation 1:

$$V_{elec} = V_{in} - \frac{incr}{2} * (e_n - 1)^2 - \left(base - \frac{incr}{2}\right) * (e_n - 1) \quad (1)$$

where V_{elec} is the voltage applied to ring electrode 'n', V_{in} is the voltage applied to the first ring electrode, 'incr' is a number added to the decrement each time the electrode number increases, and 'base' is the voltage difference between the first and second electrodes. Values for 'base' were determined by rearranging equation 1 and setting e_n = 101 (ion collection electrode) as described by equation 2:

$$base = \frac{V_{in} - V_{101} - \frac{incr}{2} * (e_n - 1)^2}{e_n - 1} + \frac{incr}{2} \quad (2)$$

where V_{101} is the voltage applied to the ion collection electrode in our system. Usable values for 'incr' depend on the number of electrodes in the stacked ring ion guide and V_{in} (e.g., for a 100-electrode stacked ring ion guide, 'incr' = 0.0, 0.1, 0.2, 0.3, 0.4, 0.5). Note that the plot is linear when incr = 0.

Similarly, the power series used in this study follows a standard power equation ($y = ax^b + c$) as described by equation 3:

$$V_{elec} = V_{in} + \frac{base}{incr - 1} * (1 - incr^{e_n - 1}) \quad (3)$$

Values for 'base' were determined by rearranging equation 3 and setting e_n = 101 as described by equation 4:

$$base = (V_{101} - V_{in}) * \frac{incr - 1}{1 - incr^{e_n - 1}} \quad (4)$$

Usable values for 'incr' for a power equation were 1.00, 1.01, 1.02, 1.03, 1.04, and 1.05. Note that incr cannot be exactly 1 for a power equation (i.e., otherwise divide by zero), so a value of $1+10^{-14}$ was used as a close alternative.

The quadratic and power voltage gradients have relatively low voltage differences between electrodes at the beginning of the gradient and higher differences at the end of the gradient. For example, a power sequence incr of 1.01 (3 kV_{in}) results in an 18 V difference between electrodes 1 and 2 and 46 V between electrodes 99 and 100. These differences are enhanced when incr is increased, meaning that high incr values create very low voltage differences between electrodes at the beginning of the device and very high differences between electrodes at the end of the device. For example, a power series incr of 1.05 establishes a 1 V difference between electrodes 1 and 2 and 137 V between electrodes 99 and 100. Similar trends are present for the quadratic sequence, although the voltage differences between electrodes are smaller compared to the power sequence. Values for V_{in} and incr were also chosen to not exceed the voltage breakdown of air (~3kV/mm) or exceed the voltage rating of common ceramic resistors (~200 V).

3.2 Ion Trajectory Simulations using Nonlinear DC Voltage Gradients

Initial ion trajectory simulations were performed using a linear voltage gradient and 3 kV_{in} (-30 V per electrode). As can be seen in Figure 2A, ions exhibited radial expansion as they traversed the stacked ring ion guide, which is expected when operating a stacked ring ion guide at atmospheric pressure and without RF confinement. Next, a quadratic voltage sequence (3 kV_{in}, incr = 0.5) was applied to the ring electrodes and ion trajectories were simulated (Figure 2B). Ions exhibited radial expansion as they traversed the first twenty ring electrodes, which is

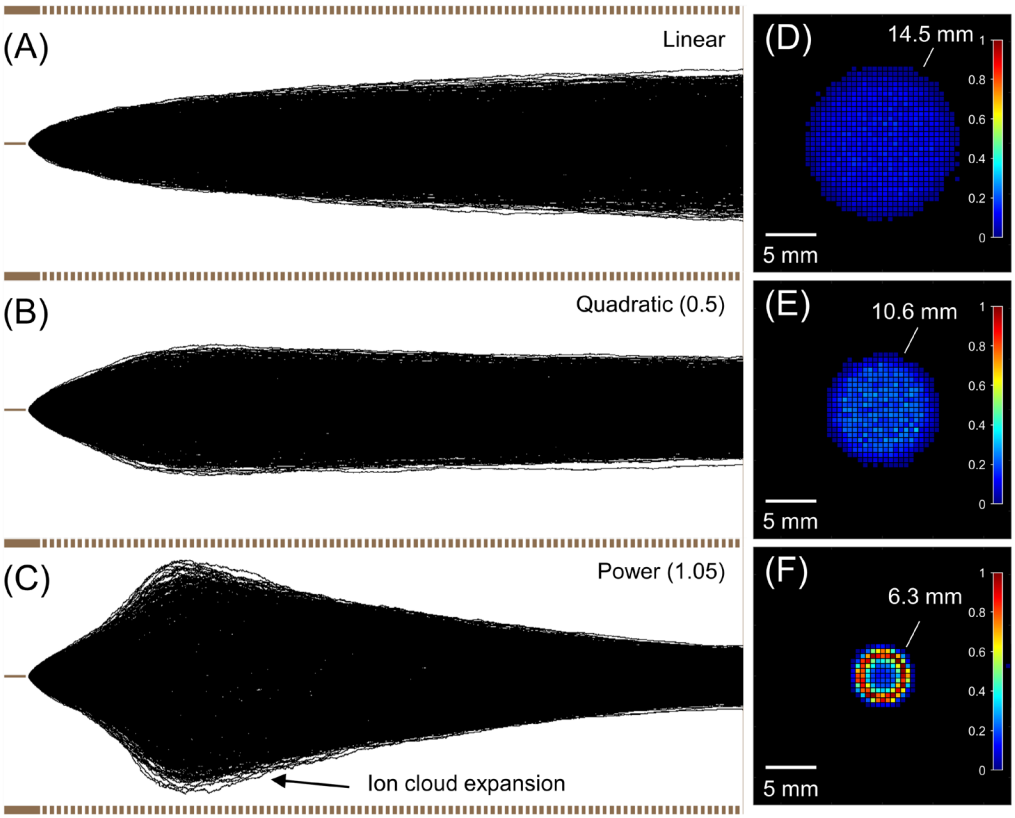

Figure 2: Ion trajectories of 1000 simulations of *m/z* 130 ions traversing a 10-cm stacked ring ion guide using (A) linear, (B) quadratic, and (C) power voltage sequences. (D,E,F) Intensity maps of 10,000 ions using each voltage sequence.

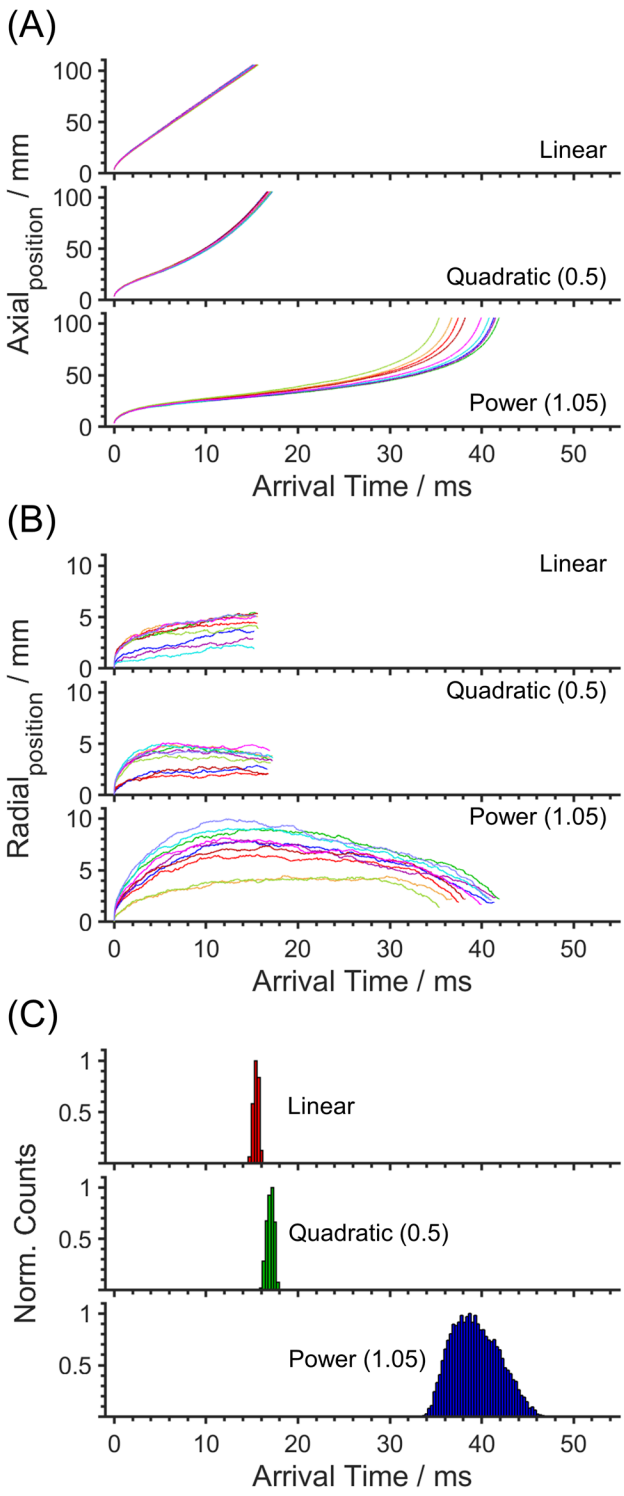

Figure 3: Plots of 10 ion simulations showing (A) ion axial position and (B) ion radial positions as a function of time of flight using linear, quadratic (0.5), and power (1.05) voltage sequences applied to a 10-cm stacked ring ion guide. (C) Simulated arrival time distributions of 10,000 ions using the three voltage sequences.

attributed to the relatively low voltage differences between adjacent electrodes (e.g., ~5 V between electrodes 1 and 2). However, ions located near the periphery of the ring electrodes began to curve inwards the farther they traveled into the device. Ions maintained their slight inward curve as they traveled through the stacked ring ion guide until reaching the detection plane. This curvature exhibited by the ions in the presence of a quadratic voltage gradient is indicative of a focusing effect at AP, and occurs without using RF. The focusing effect is attributed to the constantly increasing voltage differences between adjacent electrodes.

Next, a power voltage sequence (3 kV_{in}, incr = 1.05) was applied to the stacked ring ion guide and ion trajectories were simulated (Figure 2C). This time, ion trajectories exhibited much greater radial expansion near the entrance of the stacked ring ion guide. This is attributed to very small voltage differences between adjacent electrodes (~1-2 V). However, the power sequence resulted in stronger ion focusing in the middle and exit of the stacked ring ion guide. The stronger focusing effect is attributed to the more rapid increase in voltage differences between adjacent electrodes towards the middle and end of the stacked ring ion guide compared to the quadratic sequence. These simulations indicate that ions can be focused using a constantly changing voltage gradient, which generates an electric field whose strength increases as a function of device length. Ions are therefore 'spatially' focused because the electric field strength changes as a function of space (i.e., device length) rather than time.

Ion intensity maps of simulated spot sizes were constructed using 2D histograms to better visualize the extent to which the nonlinear voltage gradients produce ion focusing (Figure 2D, Figure 2E, Figure 2F). The intensities of the bins in all three histograms were normalized to the bin with the highest intensity (i.e., one of the bins from the power voltage sequence). Red and blue bins indicate larger and lower numbers of

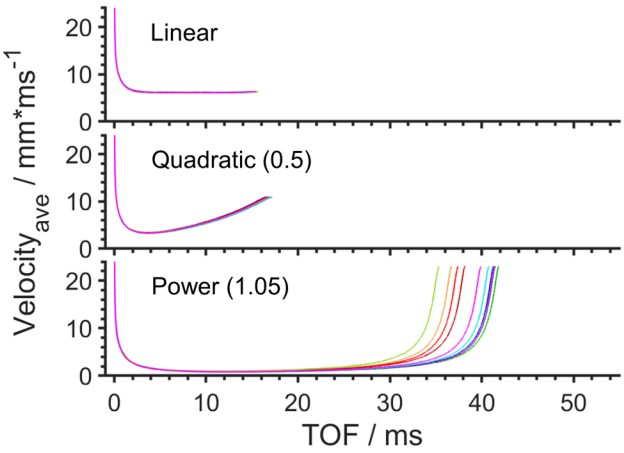

Figure 4: Plots of the average velocities of 10 ions versus time under the influence of linear, quadratic, and power voltage sequences.

ions, respectively. As can be seen, the linear, quadratic (0.5), and power (1.05) voltage sequences yielded average spots with diameters of 14.5 mm, 11.2 mm, and 6.3 mm, respectively, clearly indicating that ions are more focused when nonlinear voltage gradients are used compared to linear voltage gradients. It is worth noting that ions exhibited significant radial expansion over the first 25 or so electrodes when using the power (1.05) voltage gradient, and while the simulations do not show any ion losses under the conditions used, the inclusion of realistic space charge effects in an experimental setting may lead to ion losses in this region.

To further understand ion motion under the influence of nonlinear voltage sequences, plots of the axial and radial positions of fifty ions as a function of arrival time were generated (Figure 3A, Figure 3B). As expected, the axial positions of all ions changed linearly with time when using a linear voltage sequence. Furthermore, all ions possessed the same axial position at each time point. Plots of ion velocity versus time are given in Figure 4 and show that ions maintain a constant velocity of ~6.2 mm/ms throughout most of the stacked ring ion guide under the influence of a linear voltage gradient, which lead to a narrow arrival time distribution (ATD) width of ≈ 0.6 ms (Figure 3C). The initial drop in ion velocity is due to the high electric field between the ion emitter and the entrance to the stacked ring ion guide. We also provide heatmaps of the positions and velocities of 100 ions in Figure 5 to illustrate ion velocity throughout the stacked ring ion guide.

In contrast, applying a quadratic voltage sequence resulted in the axial positions of the ten ions changing approximately quadratically with time. Ions spent slightly more than 10 ms traversing the first 50 mm of the stacked ring ion guide and only about 7 ms to traverse the remaining 50 mm (see Figure 3A). This means that ions initially possess a lower velocity at the beginning of the stacked ring ion guide (~3.4 mm/ms) and then accelerate to a higher velocity (up to ~10.9 mm/ms) as they propagate across the device. However, all ions possessed approximately the same velocities at each time point, which also lead to a relatively narrow ATD width of ≈ 0.6 ms (see Figure 3C). We note that the change in ion velocity versus time for the quadratic sequence is approximately linear (see Figure 4).

Alternatively, changes in ion velocity were more pronounced when the power (incr = 1.05) voltage sequence was applied. The axial positions of all ten ions increased at a small but steady rate for ~26 ms and then rapidly changed until the end of the stacked ring ion guide was reached (see Figure 3A). However, each ion began to rapidly traverse the device at different time points, which is indicated by the separation of the ion packet and a wide arrival time distribution (distribution width ≈ 6.5 ms). Ion velocities were quite low (~1-2 mm/ms) for most of the time ions spent in the device. However, ion velocities rapidly became very high (up to ~23 mm/ms) near the exit of the stacked ring ion guide, though ions accelerated to this velocity at different time points.

To understand why ions reached the end of the device at different times, plots of ion radial position as a function of time were evaluated (Figure 3B). As can be seen, ion radial positions steadily increased as a function time when using a linear voltage sequence, and ions closer to

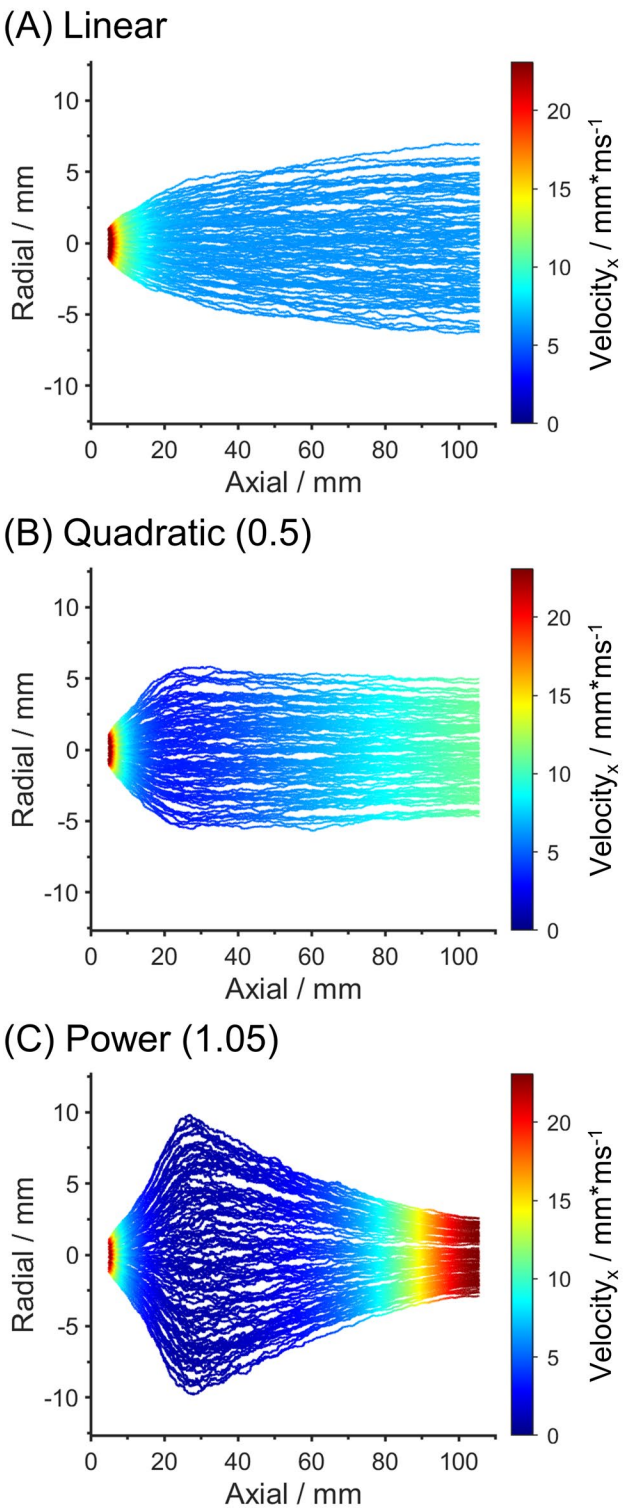

Figure 5: Reconstructed heatmaps of 100 ions depicting ion velocities at each position along a 10-cm stacked ring ion guide using (A) linear, (B) quadratic (0.5), and (C) power (1.05) voltage sequences.

the device center (i.e., radial position close to 0 mm) moved with approximately the same velocity as ions located farther away from the center. However, different behavior was observed for ions in the presence of a quadratic voltage sequence. By 2 ms, ions had separated into two groups: one group located 1 to 2 mm away from the center (red, blue, dark red traces), and one group located 3 to 4.5 mm away from the center (all other traces). The radial positions of most ion remained relatively constant throughout the rest of the simulation, although some ions moved slightly farther away from the center (e.g., red trace) while other ions moved closer (e.g., light blue trace). These results show that the quadratic voltage sequence produces a radial focusing effect at AP. However, all ten ions still moved with about the same velocities regardless of their radial distance away from the device center, meaning that the arrival time distribution was still relatively narrow.

The largest difference among the three voltage sequences can be observed in plots of ion radial position versus time when using the power (1.05) sequence. In this case, ions exhibited radial positions that varied widely. Two ions remained within 5 mm of the device center throughout the simulation (light green, orange traces) while one ion traveled out to ~10 mm away from the center (light purple trace). However, ions that did not initially move far from the center reached the end of the simulation earlier than ions that exhibited radial expansion. This can be rationalized by considering that ions at the center ideally move in a straight line towards the end of the device, but ions that exhibit radial expansion near the beginning move in an arc-like geometry. Ions traversing the length of an arc take longer to reach the end of the device than ions traveling in a straight line.

The main effect of ions spending longer times at a farther distance away from the device center is more easily observed in plots of the ATDs of 10,000 ions under the influence of all three voltage sequences (Figure 3C). ATDs from the linear and

quadratic (0.5) voltage sequences are relatively narrow, and the average arrival time (μ) for the quadratic sequence (μ ≈ 17.0 ms) is slightly greater than the linear (μ ≈ 15.4 ms). This is attributed to the fact that the electric field strength is weaker at the beginning of the stacked ring ion guide than at the end, and these differences cause ions to move slower on average compared to when a constant electric field strength is used. The standard deviation of the quadratic ATD (1σ ≈ 0.4 ms) is also slightly wider than the standard deviation of the linear ATD (1σ ≈ 0.3 ms), which is attributed to the initial radial expansion exhibited by some ions. In contrast, the average ATD of the power sequence (μ ≈ 39.4 ms) is more than double the average ATD of linear and quadratic sequences, and the standard deviation (1σ ≈ 2.6 ms) is about 10x greater than the linear sequence. The large ATD shift is attributed to the fact that the electric field strength throughout most of the stacked ring ion guide is much weaker compared to the end, and this weak electric field causes ions to move slowly throughout most of the stacked ring ion guide. Additionally, ions with widely varying radial positions will reach the end of the device at different times, and this manifests as tailing.

While all simulations described previously were performed using 3 kV_{in} and a linear, quadratic (0.5), or power (1.05) voltages, it is possible to change the slope of the nonlinear gradients as well as V_{in}. To further characterize the effect of using nonlinear DC gradients to focus ions at AP, a systematic study was performed using six different incr values for the quadratic (0.0 - 0.5) and power (1.00 – 1.05) voltage sequences and three different V_{in} values (2 kV, 3 kV, 4 kV). Ion trajectory plots are shown in Figure 6 and Figure 7, and intensity maps are shown in Figure 8 and Figure 9. The two main observations are: (1) using higher incr values (for both voltage sequences) causes ions to exhibit more radial expansion at the beginning of the stacked ring ion guide, but also exhibit stronger focusing as they traverse the device, and (2) using higher V_{in} results in narrower ion plumes, but V_{in} by itself does not cause radial ion focusing. Out of the thirty-six simulations, the smallest spot size obtained was ~5.5 mm using the power (1.05) sequence and 4 kV_{in}. While most combinations of V_{in} and incr demonstrate that nonlinear voltage gradients cause ion focusing at AP, not all combinations are desirable. For example, using 2 kV_{in} and incr = 0.5 for the quadratic gradient results in a positively increasing voltage gradient at the beginning of the stacked ring ion guide (e.g., $elec_1$ = 2000 V, $elec_2$ = 2005 V), which is not ideal. In another example, using 2 kV_{in} and incr = 1.05 for the power sequence shows ion losses at the beginning of the device caused by radial expansion. Ion losses could be mitigated by increasing V_{in}, though in practice voltage can only be increased until the breakdown potential of the background gas is reached.

One noteworthy observation from these systematic studies is that nonlinear voltage gradients with low incr and V_{in} values can produce spot sizes that linear voltage gradients can only achieve if V_{in} is made very large. For example, using a linear voltage gradient with 4 kV_{in} yields a spot size of ~13.2 mm, but a quadratic gradient using 2 kV_{in} and incr = 0.3 yields a smaller spot of ~12.6 mm. Results such as this show that nonlinear voltage gradients can achieve better ion transmission efficiencies with lower voltages than linear voltage gradients can with higher voltages. This is desirable from an experimental standpoint where equipment ratings, safety, and electrical breakdown must be considered.

Simulations were also performed using larger ions (*m/z* 2722), and bar plots of the simulated spot sizes obtained for *m/z* 130 and 2722 using 3 kV_{in} and quadratic (0.5) and power (1.05) voltage sequences are given in Figure 10. The data show similar spot sizes for both ions, meaning the nonlinear DC voltage sequences do not appear to discriminate based on ion mobility.

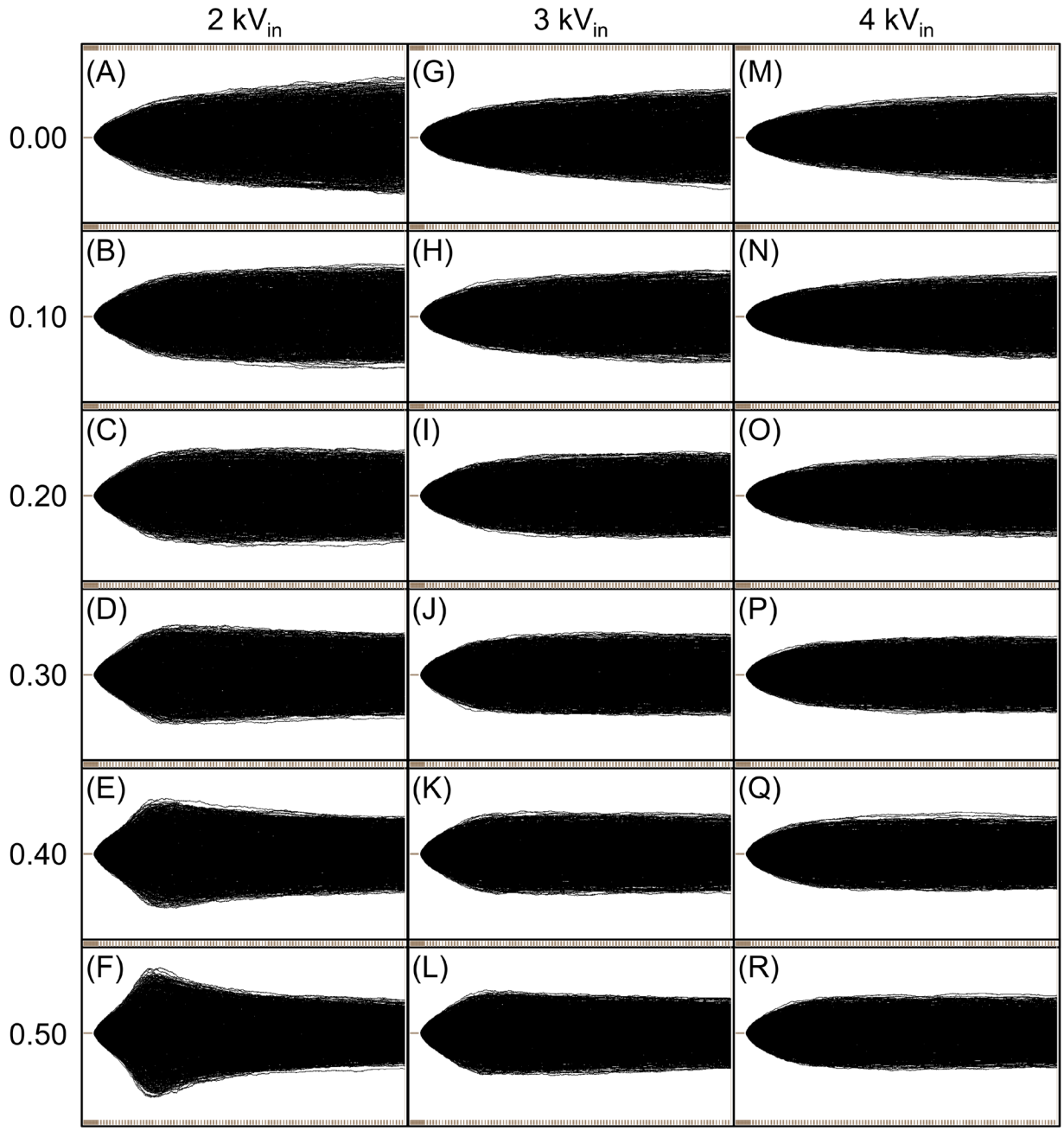

Figure 6: Ion trajectory plots of 1000 *m/z* 130 ions traversing a 10-cm stacked ring ion guide using quadratic voltage sequences with V_{in} values of (A-F) 2 kV, (G-L) 3 kV, and (M-R) 4kV, and incr values of 0.0, 0.1, 0.2, 0.3, 0.4, and 0.5.

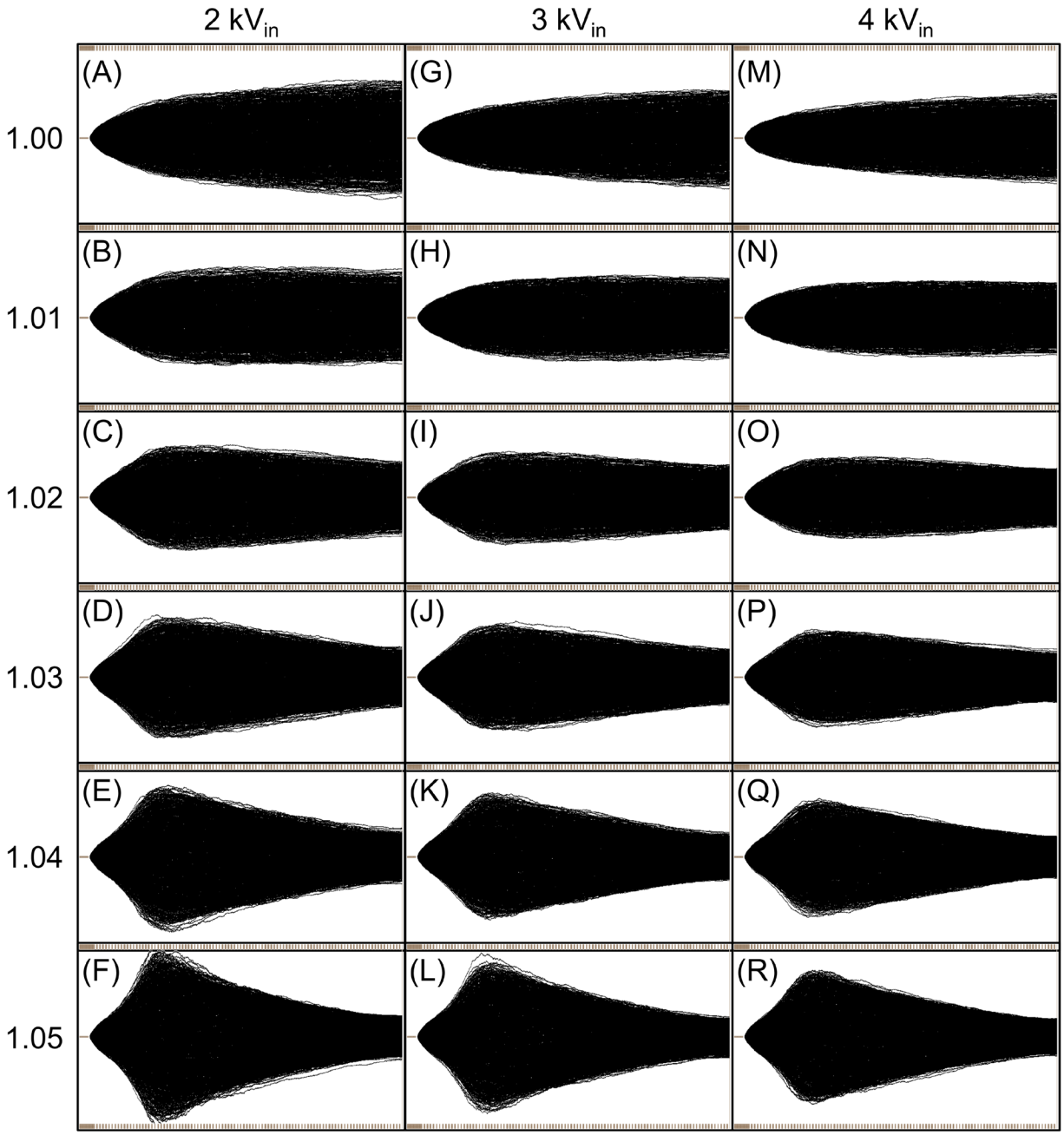

Figure 7: Ion trajectory plots of 1000 *m/z* 130 ions traversing a 10-cm stacked ring in guide using power voltage sequences with V_{in} values of (A-F) 2 kV, (G-L) 3 kV, and (M-R) 4kV, and incr values of 1.00, 1.01, 1.02, 1.03, 1.04, and 1.05.

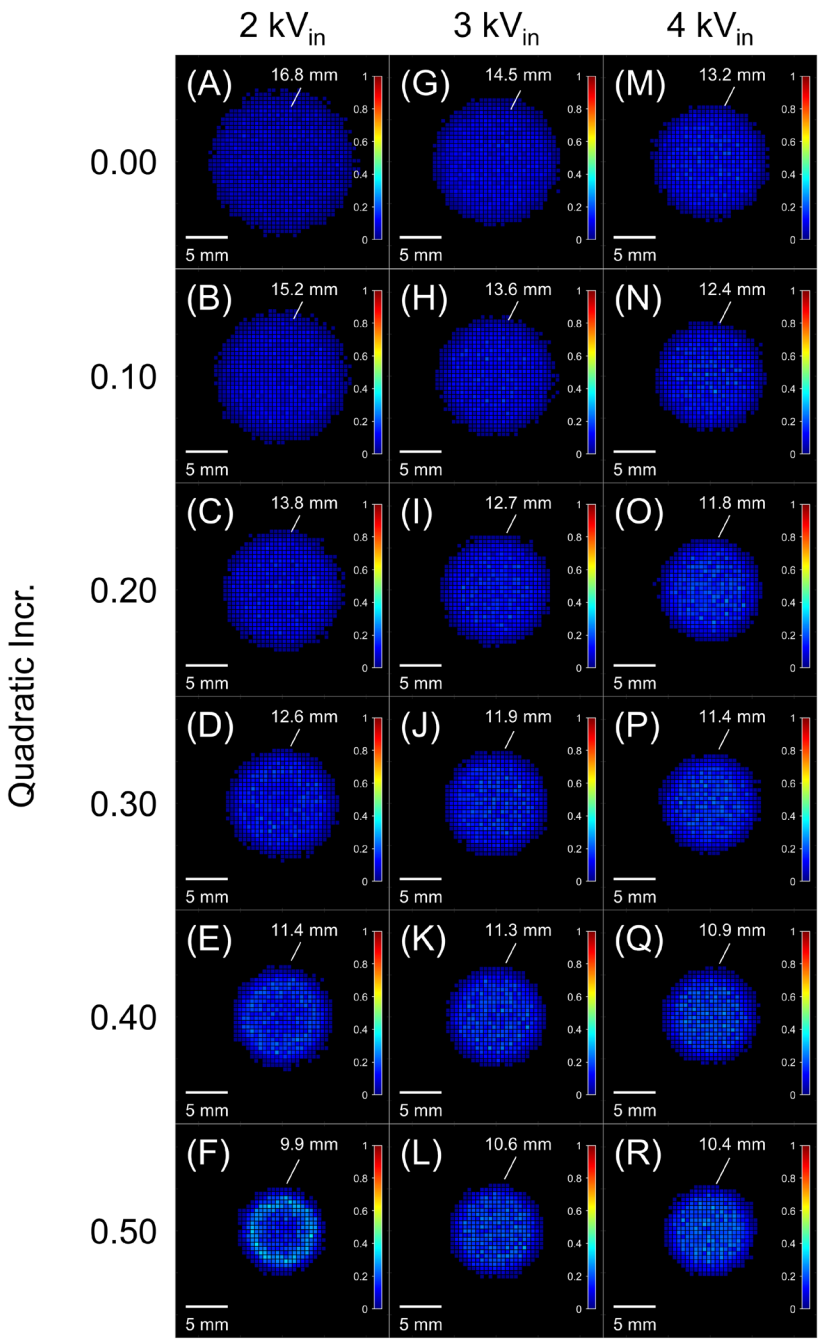

Figure 8: Normalized intensity maps of 10,000 ions and measured spot sizes using quadratic incr values of 0.0, 0.1, 0.2, 0.3, 0.4, 0.5, and V_{in} of 2kV, 3kV, 4kV.

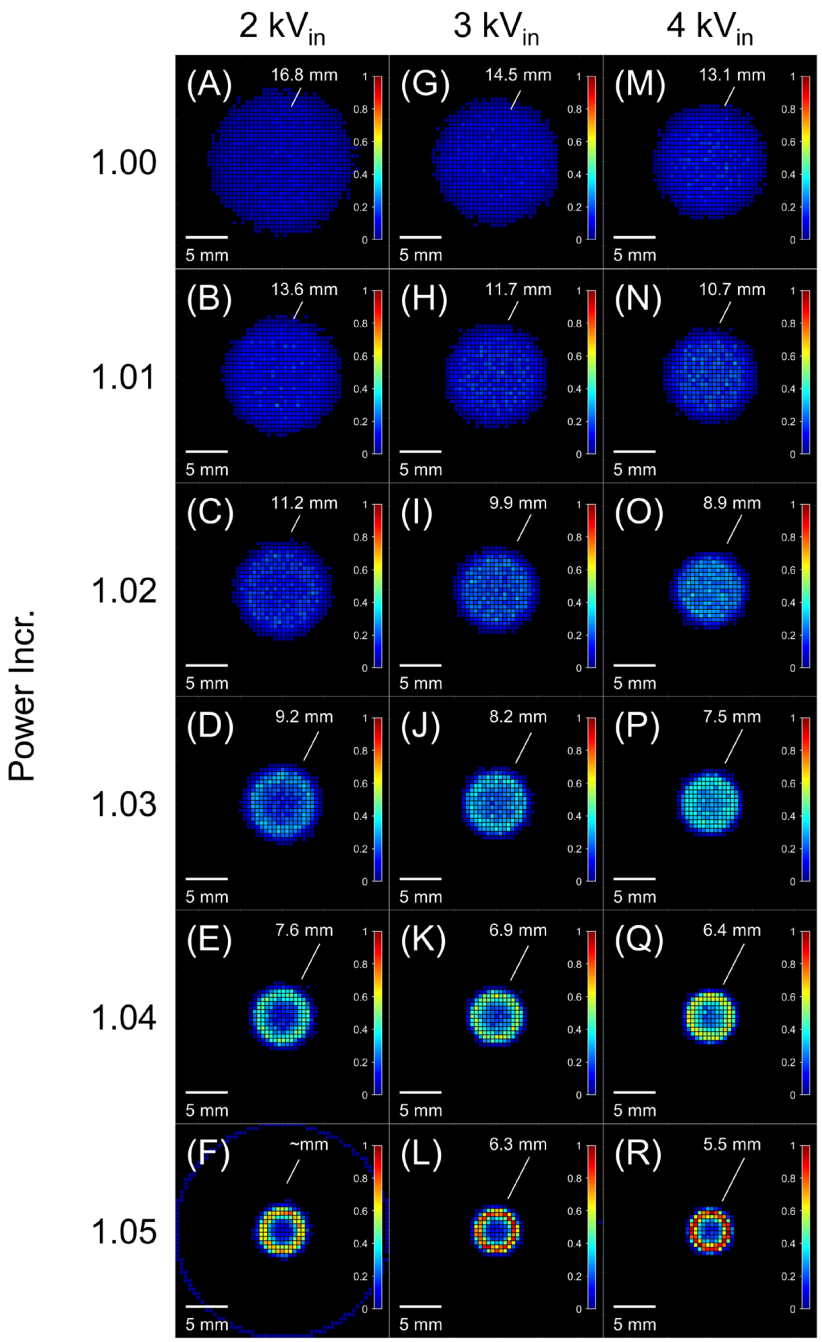

Figure 9: Normalized intensity maps of 10,000 ions and measured spot sizes using power incr values of 1+1E-14, 1.01, 1.02, 1.03, 1.04, 1.05, and V_{in} of 2kV, 3kV, 4kV.

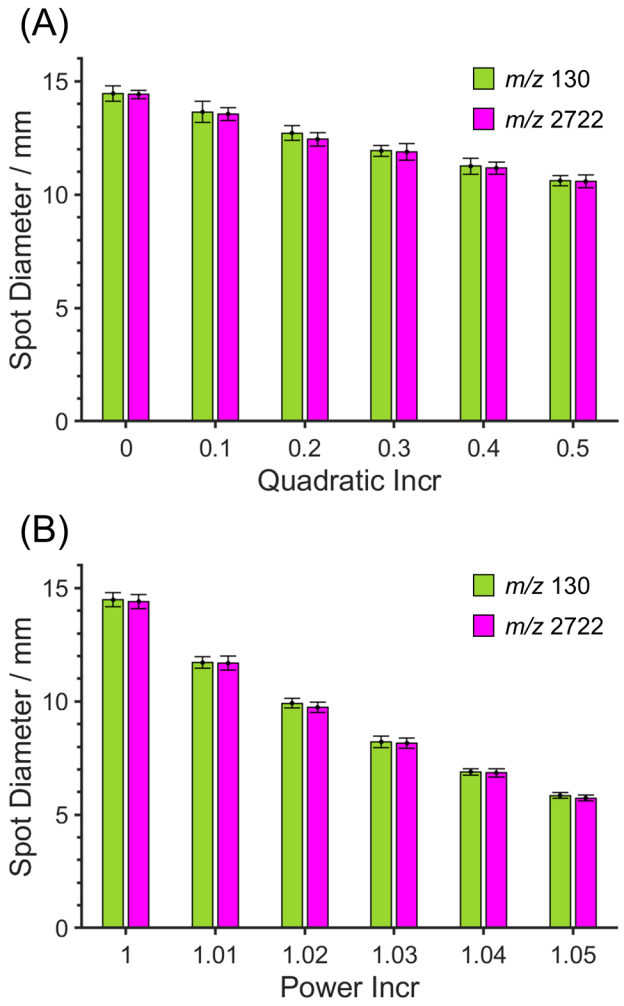

Figure 10: Simulated average spot diameters of 10,000 ions with *m/z* 130 (green bars) and *m/z* 2722 (pink bars) using (A) quadratic (0.0,0.1,0.2,0.3,0.4,0.5) and (B) power (1.00,1.01,1.02,1.03,1.04,1.05) voltage sequences. A total of 10 simulations were performed, each using 1,000 ions. Simulations using different *m/z* were performed separately. Average spot diameters were calculated as the average of these 10 runs, and errorbars represent 1 standard deviation about the average. Space charge = 2E-12C.

3.3 Curved Potential Contour Lines

To understand why nonlinear voltage gradients cause ions to focus at AP, we generated and examined plots of electric potential contour lines for the linear, quadratic (0.5), and power (1.05) voltage sequences. As can be seen, the contour lines for the linear sequence (Figure 11A) were mostly vertical. Since ions generally move perpendicular to contour lines, the presence of vertical lines indicates that radial expansion in a linear voltage gradient occurs because of thermal motion and space charge, not the electric field. In contrast, the contour lines for the quadratic sequence (Figure 11B) exhibit an outwards curvature near the device entrance. This curvature indicates that the electric field now affects ion radial motion, whereas it didn't with a linear voltage gradient. Additionally, a vertical line can be observed around the 16th electrode, suggesting an inflection point in the electric field gradient. After the 16th electrode, the contour lines begin to curve inwards, which means the electric field is now causing ions to move towards the center of the stacked ring ion guide. The curvature of the contour lines

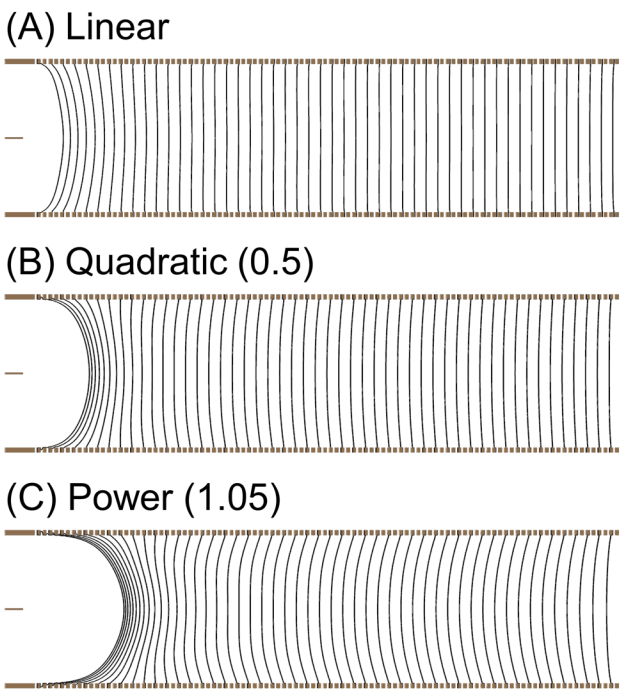

Figure 11: Electric potential contour lines in a stacked ring ion guide obtained after applying (A) linear, (B) quadratic (0.5), and (C) power (1.05) voltage sequences

increases as the exit of the device is approached, suggesting that stronger focusing occurs towards the end of the stacked ring ion guide when using a quadratic voltage gradient. The power sequence also generated contour lines that curved outwards and inwards near the device entrance and exit, respectively (Figure 11C). However, the contour lines generated by power sequence were much more curved than the lines generated by the quadratic sequence. The greater curvatures explain why the power sequence exhibits stronger ion focusing (and also defocusing) effects. We reiterate that these curved electric fields are the product of applying nonlinear DC voltage gradients rather than using curved electrodes or other geometric modifications to focus ions at AP.

3.4 Experimental Implementation of Nonlinear DC Voltage Gradients

To experimentally validate the ion focusing effects observed in the simulations, we constructed a 10-cm stacked ring ion guide comprised of 100 ring electrodes (25.4 mm i.d., 0.5 mm thickness) spaced 0.5 mm apart and applied different voltage sequences to the ion guide using custom voltage divider circuits. We electrosprayed a solution of tetraalkylammonium cations (TAAs) since they do not readily fragment and are unlikely to exhibit significant clustering. Ion current measurements were performed using a segmented Faraday cup detector. Experiments were performed by measuring the ion current at each individual ring one at a time. All measurements were performed in triplicate to obtain error bars representing 1 standard deviation about the average. The input voltage was 3 kV_{in} for all three experiments. The position of the nESI emitter and the focusing electrode voltage were optimized to obtain maximal ion current. Note that no gas flow was used in this study, meaning that any focusing effects could be directly attributed to the nonlinear DC voltages.

Plots of normalized ion current (i.e., ion current divided by ring area) versus ring number using linear, quadratic (0.5), and power (1.05) voltage gradients are shown in Figure 12. We report the y-axis as ion current (I) divided by ring area (A) because each concentric ring possesses a different area than the other rings, and wider rings are larger targets than smaller rings. The raw current measurements obtained at each concentric ring are provided in Figure 13. The data was also baseline subtracted prior to normalization. Note that the center pad of the detector is denoted on the left side of the plot and the outermost ring on the right of Figure 12. For easier visualization, the three insets at the top of Figure 5 show reconstructed ion intensity maps using the same data. As can be seen, a linear voltage gradient (red trace)

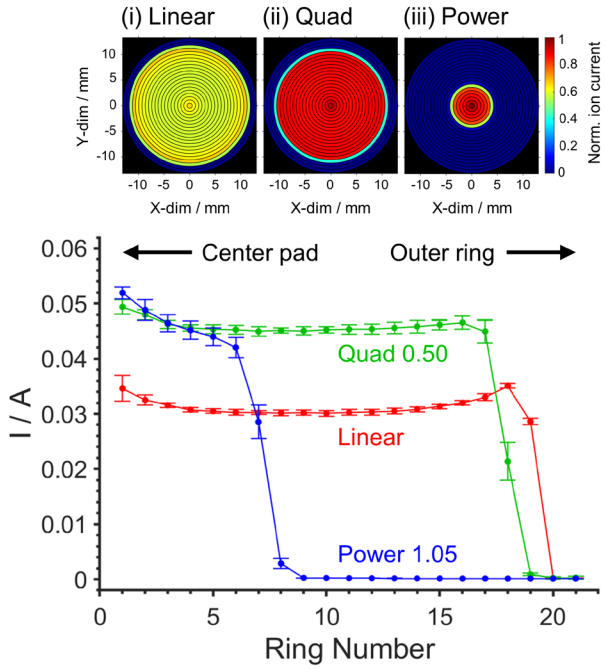

Figure 12: (A) Normalized experimental ion current measurements of tetraalkylammonium cations (C_2 – C_8) as a function of ring number using (red) linear, (green) quadratic (0.5), and (blue) power (1.05) voltage sequences. Measurements were performed in triplicate, and errorbars represent 1 standard deviation. Insets show reconstructed heatmaps of normalized experimental ion current measurements using (i) linear, (ii) quadratic (0.5), and (iii) power (1.05) voltage sequences.

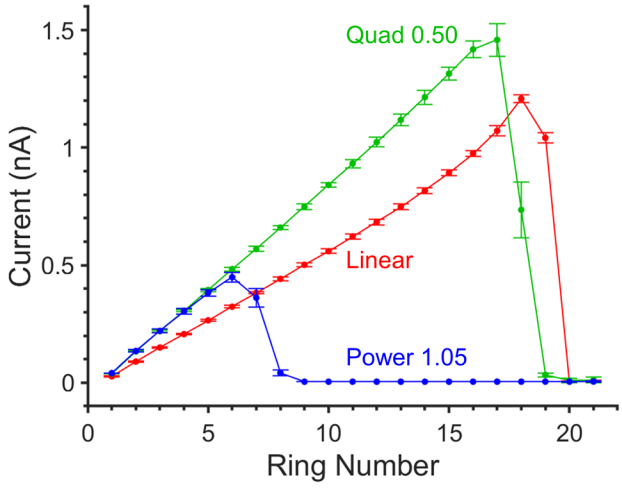

Figure 13: Unnormalized experimental current measurements using (red) linear, (green) quadratic (0.5), and (blue) power (1.05) voltage gradients. Data was baseline subtracted.

produced a normalized ion current of ~0.030 – 0.035 nA/mm^2 over the first 18 detector rings. A lower normalized ion current of ~0.028 nA/mm^2 was observed at ring 19, and zero current was obtained for rings 20 and 21. Since ion current was detected across most of the detector, this result is consistent with a device that does not exhibit any ion focusing effects, which is expected when using a linear voltage gradient.

On the other hand, experiments using a quadratic (0.5) voltage gradient produced a normalized ion current of ~0.045 nA/mm^2, which is roughly 25% higher than the linear voltage gradient. Ion current was also detected at 18 rings, which is one ring fewer than obtained with the linear gradient and corresponds to a spot size of ~22.4 mm. The difference in experimental spot size between the linear and quadratic (0.5) gradients was ~1.3 mm, which is smaller than the expected 3.9 mm reduction achieved with simulations. This discrepancy in spot size is likely due to the inability to accurately simulate space charge repulsion among very large numbers of ions in one simulation. The main point is that the quadratic gradient produces a higher experimental ion current and a smaller spot size, which experimentally demonstrates the ability to focus ions at AP using a nonlinear voltage gradient.

Lastly, a power (1.05) voltage gradient was applied to the stacked ring ion guide and a normalized ion current of ~0.042 – 0.052 nA/mm^2 was obtained. Ion current was detected on the 7 innermost rings, which corresponded to a spot size of ~8.6 mm. Interestingly, the normalized ion current at the middle pad was 0.052 nA/mm^2, which was the largest value out of any of the ion current measurements (i.e., linear, quadratic, power). This observation indicates that the power voltage gradients causes an AP ion focusing effect. The normalized ion current on rings 2 through 7 were roughly the same, though they were slightly lower than obtained at the center pad. Interestingly, the ion current sharply dropped at ring 8, and no ion current was detected at rings 9 through 21. While this

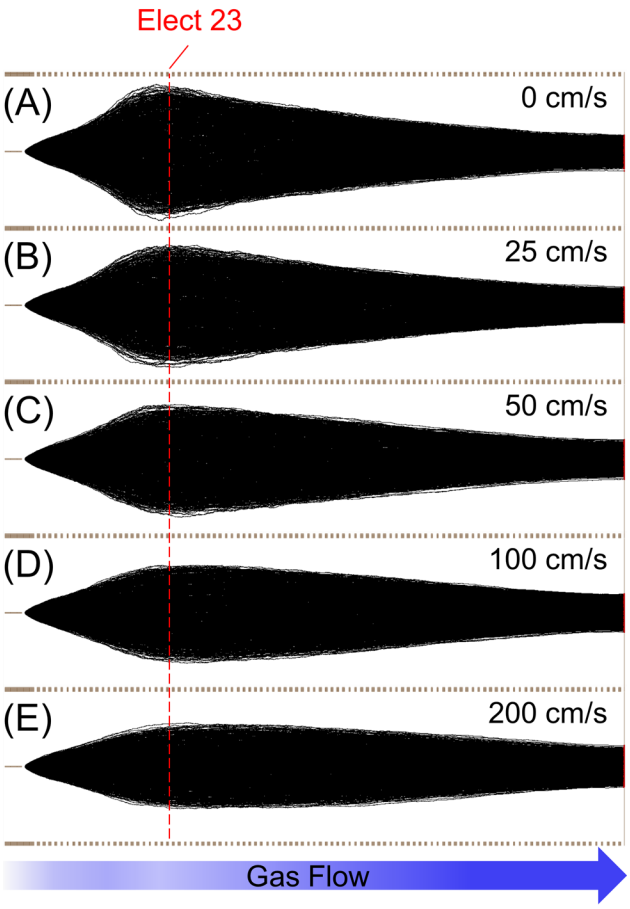

Figure 14: Ion trajectories of 1000 ions (*m/z* 130; K_0 = 1.88 cm^2/Vs) obtained using a power (1.05) voltage sequence and gas flow velocities of (A) 0, (B) 25, (C) 50, (D) 100, and (E) 200 cm/s. (F) Overlaid plots of ion plume widths measured at electrode 23 (red dashed trace) and the collection plate (black solid trace) using 10,000 ions. Errorbars represent 1 standard deviation about the average ion plume width. V_{in} = 3 kV.

observation means that the power sequence yielded a spot size of ~8.7 mm, the overall ion current was ~10x lower compared to a linear gradient. The losses associated with the power voltage gradient can be rationalized by considering that simulations show ion radial expansion due to the small voltage gradient at the beginning of the power voltage sequence, and ion losses are observed in the simulations using 2 kV_{in} and incr = 1.05. This result indicates that power voltage gradients, like quadratic voltage gradients, cause ions to focus at AP; however, the power voltage gradient evaluated in this study only focused ions that originated near the center of the ring electrodes.

We note it is unlikely that our nonlinear voltage gradients cause ions to gain enough internal energy to fragment since ions rapidly cool at AP due to the large number of collisions they experience over a short distance. Although the largest voltage drop we used was ~150 V across 0.5 mm (not uncommonly large), future studies with labile compounds and a mass spectrometer will monitor for any ion fragmentation effects.

3.5 Simulating gas flows combined with nonlinear DC voltage gradients

While the quadratic voltage gradient showed the highest ion currents in experiments, the power voltage gradient has the potential to produce even larger ion currents at AP if early ion losses due to low electric field strength can be overcome. To address these early ion losses, we used simulations to study how adding a gas flow to a power (1.05) voltage sequence affected ion radial motion. SIMION's SDS collision model was used to incorporate a laminar gas flow running in the same direction as ion motion. Ion trajectory simulations were performed using gas flow velocities of 0, 25, 50, 100, and 200 cm/s (0.0, 7.6, 15.2, 30.4, and 60.8 L/min, respectively; cross sectional area = 25.4 mm).

Plots of the ion trajectories obtained using a power (1.05) voltage sequence and gas flow rates of 0 to 200 cm/s are shown in Figure 14. As can be seen, all simulated gas velocities caused the widths of the ion plumes near the entrance of the device to decrease. This means that gas flows successfully kept ions away from the surfaces of the ring electrodes in regions of low electric field strength, which is the main reason ions are lost when using a high order power voltage gradient and no gas flow. Additionally, the power (1.05) voltage gradient was strong enough near the end of the device to focus ions to small spots even with a gas flow being present. These simulations show that combining gas flows and nonlinear voltage gradients should provide a way to strongly focus ions near the end of a stacked ring ion guide while minimizing losses occurring near the entrance. It is worth noting that the final spot sizes of ions slightly increased when gas flows were introduced (Figure 14F, black trace). However, the widths of the ion plumes at their widest point (around electrode 23) were much smaller when gas flows were used compared to when gas flows were not used (Figure 14F, red trace). Such a large decrease in ion plume width near the device entrance is desirable because high order power voltage gradients should focus ions more strongly than any linear or quadratic voltage gradients.

We also performed a set of ion trajectory simulations that utilized a wide starting distribution of ions and no ESI emitter in addition to gas flows. Simulations were performed using a power (1.05) voltage gradient and the same gas flow velocities used previously. Ion trajectories are shown in Figure 15 along with a plot of final spot sizes. For comparison, simulations were also performed using a linear voltage gradient. As can be seen, ion trajectories obtained with the power voltage gradient were once again narrower than those obtained with the linear voltage gradient. Similar to the previous set of simulations, adding gas flows caused the final spot sizes of both voltage gradients to slightly increase compared to when no gas flow was present. However, the overall focusing effect of the power voltage gradient was still strong enough to overcome the strength of the gas flow near the exit of the stacked ring ion guide. This study once again confirms that combining a gas flow with a nonlinear voltage gradient still yields a small spot size while likely reducing ion losses associated with radial expansion near the entrance of the stacked ring ion guide.

Based on these simulations, we expect that introducing gas flows is one viable way to overcome early ion losses associated with nonlinear voltage gradients. We note that the SDS model in SIMION only simulates a uniformly flowing gas and additional simulations using more accurate gas flow models (i.e., incorporating flow fields) are needed to a clearer picture of ion motion in flowing gases. However, future experiments will explore combining gas flows and nonlinear voltage gradients to further improve ion transmission at AP.

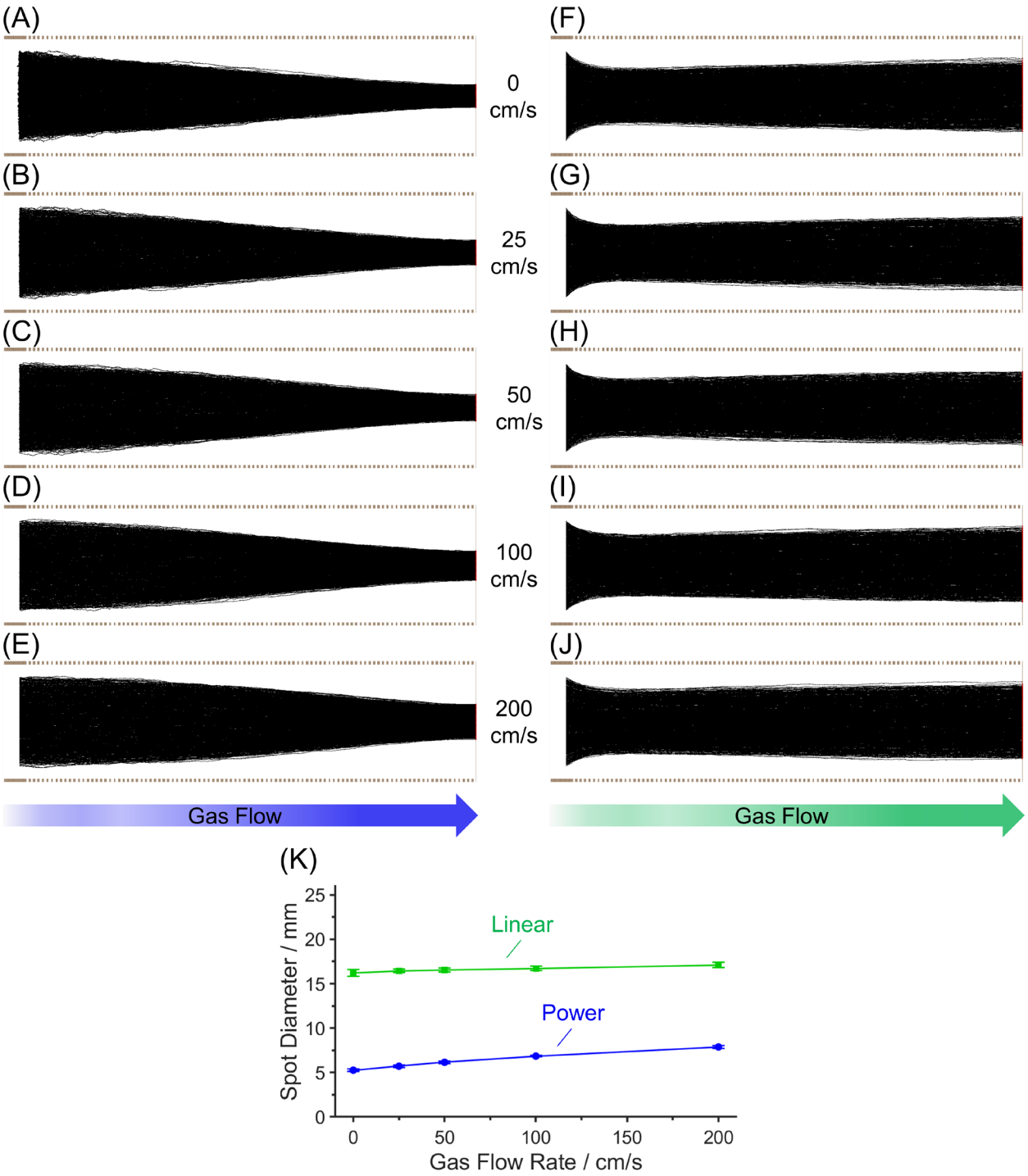

Figure 15: Ion trajectories of 1000 ions obtained using a wide starting distribution, no emitter, and gas flow velocities of (A,F) 0, (B,G) 25, (C,H) 50, (D,I) 100, and (E,J) 200 cm/s. Ion trajectories shown in the left (A-E) and right (F-J) columns were acquired a using power (1.05) and linear voltage sequences, respectively. (K) Plots of ion plume widths measured at the collection plate using 10,000 ions. Errorbars represent 1 standard deviation about the average ion plume width. V_{in} = 3 kV. The focusing electrode was kept at +5 V above V_{in}.

4.0 Conclusions

Nonlinear DC voltage sequences were theoretically and experimentally shown to focus ions in the open air when applied to a 10-cm stacked ring ion guide. Nonlinear voltage sequences produce curved electric field lines that pointed towards the center of the device, resulting in ion focusing. This focusing effect was strong enough to overcome ion diffusion at AP and demonstrates a new way of overcoming ion diffusion at elevated pressures. Although the voltage sequences used here followed unaltered mathematical functions, it may be possible to tailor voltage sequences (e.g., splice different functions together) to minimize radial expansion near the beginning of the stacked ring ion guide. Similarly, introducing a small gas flow running parallel to ion motion may help minimize early ion losses and lead to a further increase in ion flux.

The ability to focus ions at AP using nonlinear electric fields over long distances will open the door for many gas-phase ion chemistry applications by providing more time for gas-phase reactions to occur, which in turn will improve reaction yields. Additionally, higher ion fluxes will increase deposition currents in AP soft landing experiments, which will reduce overall collection times.

5.0 References

Allen, Samuel J. and Matthew F. Bush. 2016. “Radio-Frequency (rf) Confinement in Ion Mobility Spectrometry: Apparent Mobilities and Effective Temperatures.” *Journal of the American Society for Mass Spectrometry* 27, no. 12 (December): 2054-2063. https://doi.org/10.1007/s13361-016-1479-9.

Anthony, Staci N., Deven L. Shinholt, and Martin F. Jarrold. 2014. “A simple electrospray interface based on a DC ion carpet.” *International Journal for Mass Spectrometry* 371, (October): 1-7. https://doi.org/10.1016/j.ijms.2014.06.007.

Badu-Tawiah, Abraham K., Chunping Wu, and R. Graham Cooks. 2011. “Ambient Ion Soft Landing.” *Analytical Chemistry* 83, no. 7 (April): 2648-2654. https://doi.org/10.1021/ac102940q.

Baird, Zane, Wen-Ping Peng, and R. Graham Cooks. 2012. “Ion transport and focal properties of an ellipsoidal electrode operated at atmospheric pressure”. *International Journal for Mass Spectrometry* 330-332, (December): 277-284. https://doi.org/10.1016/j.ijms.2012.09.009.

Baird, Z.; Pu Wei, and R. Graham Cooks. 2015. “Ion creation, ion focusing, ion/molecule reactions, ion separation, and ion detection in the open air in a small plastic device.” *Analyst* 140, no 3 (November): 696-700. https://doi.org/10.1039/C4AN01929F.

Bush, Matthew F., Zoe Hall, Kevin Giles, John Hoyes, Carol V. Robinson, and Brandon T. Ruotolo. 2010. “Collision Cross Sections of Proteins and Their Complexes: A Calibration Framework and Database for Gas-Phase Structural Biology.” *Analytical Chemistry* 82, no. 22 (November): 9557-9565. https://doi.org/10.1021/ac1022953.

Deng, Liulin, Yehia M. Ibrahim, Ahmed M. Hamid, Sandilya V. B. Garimella, Ian K. Webb, Xueyun Zheng, Spencer A. Prost, et al. 2016. “Ultra-High Resolution Ion Mobility Separations Utilizing Traveling Waves in a 13 m Serpentine Path Length Structures for Lossless Ion Manipulations Module.” *Analytical Chemistry* 88, no. 18 (September): 8957-8964. https://doi.org/10.1021/acs.analchem.6b01915.

Deng, Liulin, Ian K. Webb, Sandilya V. B. Garimella, Ahmed M. Hamid, Xueyun Zheng, Randolph V. Norheim, Spencer A. Prost, et al. 2017. “Serpentine Ultralong Path with Extended Routing (SUPER) High Resolution Traveling Wave Ion Mobility-MS using Structures for Lossless Ion Manipulations.” *Analytical Chemistry* 89, no. 8 (April): 4628-4634. https://doi.org/10.1021/acs.analchem.7b00185.

Douglas, Donald J. 2009. “Linear quadrupoles in mass spectrometry.” *Mass Spectrometry Reviews* 28, no. 6 (June): 937-960. https://doi.org/10.1002/mas.20249.

Fort, Kyle L, Joshua A. Silveira, and David H. Russell. 2013. “The Periodic Focusing Ion Funnel: Theory, Design, and Experimental Characterization by High-Resolution Ion Mobility-Mass Spectrometry.” *Analytical Chemistry* 85, no 20 (October): 9543-9548. https://doi.org/10.1021/ac401629b.

Garimella, Sandilya V. B., Wei Xu, Guangming Huang, Jason D. Harper, R. Graham Cooks, and Zheng Ouyang. 2012. “Gas-flow assisted ion transfer for mass spectrometry.” *Journal of Mass Spectrometry* 47, no 2 (February): 201-207. https://doi.org/10.1002/jms.2955.

Gillig, Kent J., Brandon T. Ruotolo, Earle G. Stone, and David H. Russell. 2004. “An electrostatic focusing ion guide for ion mobility-mass spectrometry.” *International Journal of Mass Spectrometry* 239, no. 1 (December): 43-49. https://doi.org/10.1016/j.ijms.2004.09.005.

Ibrahim, Yehia M., Keqi Tang, Aleksey V. Tolmachev, Alexandre A. Shvartsburg, and Richard D. Smith. 2006. “Improving Mass Spectrometer Sensitivity Using a High-Pressure Electrodynamic Ion Funnel Interface.” *Journal of the American Society for Mass Spectrometry* 17, no. 9 (September): 1299-1305. https://doi.org/10.1016/j.jasms.2006.06.005.

Iyer, Kiran, Brett M. Marsh, Grace O. Capek, Robert L. Schrader, Shane Tichy, and R. Graham Cooks. 2019. “Ion Manipulation in Open Air Using 3D-Printed Electrodes.” *Journal of the American Society for Mass Spectrometry* 30, no. 12 (December): 2584-2593. https://doi.org/10.1007/s13361-019-02307-2.

Karpas, Z., G. A. Eiceman, R. G. Ewing, A. Algom, R. Avida, M. Friedman, A. Matmor, and O. Shahal. 1993. “Ion distribution profiles in the drift region of an ion mobility spectrometer.” *International Journal of Mass Spectrometry Ion Processes* 127, (August): 95-104. https://doi.org/10.1021/acs.analchem.7b04586.

Kelly, Ryan T. Aleksey V. Tomachev, Jason S. Page., Keqi Tang, and Richard D. Smith. 2010. “The ion funnel: theory, implementations, and applications.” *Mass Spectrometry Reviews* 29, no. 2 (April): 294-312. https://doi.org/10.1002/mas.20232.

Kolomiets, Yuri N. and Viktor V. Pervukhin. 2011. “Atmospheric pressure ion focusing with a vortex stream.” *Talanta* 85, no. 4 (September): 1792-1797. https://doi.org/10.1016/j.talanta.2011.07.005

Kottke, Peter A., Jung Y. Lee, Alex P. Jonke, Chinthaka A. Seneviratne, Elizabeth S. Hecht, David C. Muddiman, Matthew P. Torres, and Adrei G. Fedorov. 2017. “DRILL: An Electrospray Ionization-Mass Spectrometry Interface for Improved Sensitivity via Inertial Droplet Sorting and Electrohydrodynamic Focusing in a Swirling Flow.” *Analytical Chemistry* 89, no. 17 (June): 8981-8987. https://doi.org/10.1021/acs.analchem.7b01555.

Mächler, Lars, Igor Filippov, and Peter J. Derrick. “Unveiling the Intricacies of the Curved-Field Ion Mirror.” *European Journal of Mass Spectrometry* 21, no. 3 (June): 115-123. https://doi.org/10.1255/ejms.1352.

Meier, Lukas, Christian Berchtold, Stefan Schmid, and Renato Zenobi. 2012. “Extractive Electrospray Ionization Mass Spectrometry—Enhanced Sensitivity Using an Ion Funnel.” *Analytical Chemistry* 84, no. 4 (February): 2076-2080. https://doi.org/10.1021/ac203022x.

Nolting, Dirk, Robert Malek, and Alexander Makarov. 2019. “Ion traps in modern mass spectrometry.” *Mass Spectrometry Reviews* 38, no. 2 (October): 150-168. https://doi.org/10.1002/mas.21549.

Salentijn, Gert IJ., Richard D. Oleschuk, and Elisabeth Verpoorte. 2017. “3D-Printed Paper Spray Ionization Cartridge with Integrated Desolvation Feature and Ion Optics.” *Analytical Chemistry* 89, no. 21 (November): 11419-11426. https://doi.org/10.1021/acs.analchem.7b02490.

Schneider, Bradley B., D. J. Douglas, and David D. Y. Chen. 2002. “An atmospheric pressure ion lens that improves nebulizer assisted electrospray ion sources.” *Journal of the American Society for Mass Spectrometry* 13, no. 8 (August): 906-913. https://doi.org/10.1016/S1044-0305(02)00389-6.

Schrader, Robert L., Brett M. Marsh, and R. Graham Cooks. 2020. “Temporal distribution of ions in ambient pressure drift tubes with turns.” *International Journal for Mass Spectrometry* 456, (October): 116391. https://doi.org/10.1016/j.ijms.2020.116391.

Shaffer, Scott A., Keqi Tank, Gordon A. Anderson, David C. Prior, Harold R. Udseth, and Richard D. Smith. 1997. “A novel ion funnel for focusing ions at elevated pressure using electrospray ionization mass spectrometry.” *Rapid Communications in Mass Spectrometry* 11, no. 16 (December): 1813-1817. https://doi.org/10.1002/(SICI)1097-0231(19971030)11:16<1813::AID-RCM87>3.0.CO;2-D

Shvartsburg, Alexandre A. and Richard D. Smith. 2008. “Fundamentals of Traveling Wave Ion Mobility Spectrometry.” *Analytical Chemistry* 80, no. 24 (December): 9689-9699.

Smith, Barry Lee, Cedric Boisdon, David Romero-Perez, Tung-Ting Sham, Behnam Bastani, Yufeng Zhou, Stephen McWillian, Abraham Kwame Badu-Tawiah, and Simon Maher. 2022. “Ambient ion focusing for paper spray ionization.” *International Journal for Mass Spectrometry* 471, (January): 116737. https://doi.org/10.1016/j.ijms.2021.116737.

Tata, Alessandra, Chiara Salvitti, and Federico Pepi. 2020. “From vacuum to atmospheric pressure: A review of ambient ion soft landing.” *International Journal for Mass Spectrometry* 450, (April): 116309. https://doi.org/10.1016/j.ijms.2020.116309

Zhou, Li, Bingfang Yue, David V. Dearden, Edgar D. Lee, Alan L. Rockwood, and Milton L. Lee. 2003. “Incorporation of a Venturi Device in Electrospray Ionization.” *Analytical Chemistry* 75, no. 21 (November): 5978-5983. https://doi.org/10.1021/ac020786e.

Pacific Northwest National Laboratory

902 Battelle Boulevard
P.O. Box 999
Richland, WA 99354

1-888-375-PNNL (7665)

www.pnnl.gov